

Increased night-time oxidation over China despite widespread decrease across the globe

Received: 26 July 2022

Accepted: 29 December 2022

Published online: 26 January 2023

 Check for updates

Haichao Wang^{1,2,3,10}, Haolin Wang^{1,3,10}, Xiao Lu^{1,3,10}, Keding Lu²✉, Lin Zhang⁴, Yee Jun Tham⁵, Zongbo Shi⁶, Kenneth Aikin^{7,8}, Shaojia Fan^{1,3}, Steven S. Brown^{8,9}✉ & Yuanhang Zhang²✉

Nitrogen oxides ($\text{NO}_x = \text{NO} + \text{NO}_2$) emitted from combustion and natural sources are reactive gases that regulate the composition of Earth's atmosphere. Nocturnal oxidation driven by nitrate radicals is an important but poorly understood process in atmospheric chemistry, affecting the lifetimes of NO_x and ozone and particulate pollution levels. Understanding the trends of nitrate radicals is important to formulating effective pollution mitigation strategies and understanding the influence of NO_x on climate. Here we analyse publicly available monitoring data on NO_x and ozone to assess production rates and trends of surface nitrate radicals from 2014 to 2021 across the globe. We show that nitrate radicals have undergone strong increases in China during 2014–2019 but exhibited modest decreases in the United States and the European Union. Accelerated night-time oxidation has shortened the lifetime of summer NO_x in China by 30% during 2014–2019. This change will strongly affect ozone formation and has policy implications for the joint control of ozone and fine particulate pollution.

Nitrate radical (NO_3) is one of the major tropospheric oxidants and thus substantially impacts atmospheric chemical cycles important to air quality and climate^{1,2}. NO_3 is primarily a night-time species that is formed by the reaction of nitrogen dioxide (NO_2) and ozone (O_3). It initiates the nocturnal oxidation of volatile organic compounds (VOCs), particularly olefins, and contributes to secondary organic aerosol (SOA) production^{3–5}. For example, NO_3 oxidation accounts for 10–20% of global SOA on average and could be more important in polluted

areas^{6–9}. It further produces particulate inorganic nitrate via dinitrogen pentoxide (N_2O_5) heterogeneous hydrolysis^{10,11}. Night-time NO_3 chemistry influences next-day photochemistry by removing nitrogen oxides (NO_x) and VOCs, main precursors of O_3 , and through formation of nitryl chloride (ClNO_2), a photochemical Cl reservoir^{12–14}. ClNO_2 acts as an important radical source and enhances the O_3 formation by up to 7.0 parts per billion by volume (ppbv) across the Northern Hemisphere¹⁵. NO_3 reactions thus act as a hub coupling the evolution of two critical

¹School of Atmospheric Sciences, Sun Yat-Sen University, and Southern Marine Science and Engineering Guangdong Laboratory (Zhuhai), Zhuhai, China. ²State Key Joint Laboratory of Environmental Simulation and Pollution Control, The State Environmental Protection Key Laboratory of Atmospheric Ozone Pollution Control, College of Environmental Sciences and Engineering, Peking University, Beijing, China. ³Guangdong Provincial Observation and Research Station for Climate Environment and Air Quality Change in the Pearl River Estuary, Key Laboratory of Tropical Atmosphere-Ocean System (Sun Yat-sen University), Ministry of Education, Zhuhai, China. ⁴Laboratory for Climate and Ocean-Atmosphere Studies, Department of Atmospheric and Oceanic Sciences, School of Physics, Peking University, Beijing, China. ⁵School of Marine Sciences, Sun Yat-sen University, Zhuhai, China. ⁶School of Geography, Earth and Environmental Sciences, University of Birmingham, Birmingham, UK. ⁷Cooperative Institute for Research in Environmental Sciences, University of Colorado, Boulder, CO, USA. ⁸NOAA Chemical Sciences Laboratory, Boulder, CO, USA. ⁹Department of Chemistry, University of Colorado, Boulder, CO, USA. ¹⁰These authors contributed equally: Haichao Wang, Haolin Wang, Xiao Lu. ✉e-mail: k.lu@pku.edu.cn; steven.s.brown@noaa.gov; yhzhang@pku.edu.cn

air pollutants (O_3 and particulate matter $\leq 2.5 \mu\text{m}$ in diameter ($\text{PM}_{2.5}$)) of major concern. Despite its importance, less attention has been paid to night-time processes than to photochemical reactions. Specifically, the present-day increasing severe O_3 in China¹⁶ and decreasing O_3 in the United States¹⁷ may cause large-scale shifts in nocturnal NO_3 chemistry and its impact in these regions, but trends in the magnitude or rates of nocturnal oxidation processes have not been well assessed as yet.

Since NO_3 has a short lifetime, its impact is regulated by its formation process. Thus, we examine the nitrate radical production rate (PNO_3 ; equation (1)) as an indicator of NO_3 oxidation capacity¹⁸, here $k_{\text{NO}_2+\text{O}_3}$ is the reaction rate of NO_2 and O_3 . We use nocturnal PNO_3 (averaged over 20:00–06:00 local standard time (LT) at each site, the approximate darker half of the diel cycle; Supplementary Fig. 1 confirms the consistency of using a local standard time filter window with local solar zenith angles time window) and its trend to assess the evolution of night-time chemistry from a global perspective on the basis of a comprehensive surface observation dataset covering China, India, the European Union and the United States over 2014–2021 (Methods). We note that there are several regions not covered in this study (such as tropical regions and Southern Hemisphere) due to the gap of monitoring network, even though it is global in scope:

$$\text{PNO}_3 = k_{\text{NO}_2+\text{O}_3} [\text{NO}_2][\text{O}_3] \quad (1)$$

Distributions and trends of PNO_3

Figure 1a shows that the average nocturnal PNO_3 in the warm season (defined as April–September) during 2018–2019 in China was $1.07 \pm 0.38 \text{ ppbv h}^{-1}$, higher than those in the United States, the European Union and India by 155%, 174% and 37%, respectively (Extended Data Table 1). Our result demonstrates that the most active night-time chemistry and strong nocturnal oxidation capacity occurs in China compared with other regions, an aspect of atmospheric oxidation that has not been recognized previously. The conventional view of night-time surface-level chemistry in polluted environments is that high NO_x emissions strongly titrate O_3 and NO_3 at night, thus suppressing NO_3 chemistry in urban areas. Unexpectedly, the regions with high PNO_3 are concentrated in urban clusters in east China, with intensive NO_x emission. The overall high surface nocturnal PNO_3 in China is determined by elevated nocturnal NO_2 and O_3 (Extended Data Fig. 1)¹⁹. In particular, the surface nocturnal NO_2 in China is about twice that of the United States and the European Union. Ground-level temperature contributes only slightly to the regional differences in PNO_3 through the temperature-dependence reaction rate term $k_{\text{NO}_2+\text{O}_3}$ (Extended Data Table 2). This term in China is similar to that of the United States (3.1×10^{-17} versus 3.0×10^{-17} molecules $\text{cm}^{-3} \text{ s}^{-1}$), since both regions span similar latitudes, but is higher in India (lower latitude and higher temperatures) and lower in the European Union (higher latitude and lower temperatures).

The PNO_3 trend in the warm season over 2014–2019 demonstrates a rapid growth of PNO_3 in China by $0.04 \text{ ppbv h}^{-1} \text{ yr}^{-1}$ (5.8%) on average, with 43.3% of sites showing positive trends with $P < 0.1$, while trends of PNO_3 in the European Union and the United States are much smaller and insignificant, with a larger fraction (47.9% in the European Union and 64.7% in the United States) of sites showing negative trends (Fig. 1c). In this Article, we estimate trends with monthly data in the warm season of 2014–2019 with the seasonal cycle and autocorrelation removed to derive robust trends even for a relatively short period¹⁷. The PNO_3 trends at the Chinese monitoring sites are overwhelmingly positive in all city clusters examined here, with large variabilities in the magnitudes of the trends (Extended Data Fig. 2 and Extended Data Table 3). By comparison, most sites in the European Union and the United States showed small increasing or decreasing trends. The diurnal pattern of PNO_3 is similar in the four regions and showed an overall change during the study period, rather than influenced by the curve shape change (Fig. 2).

We found that the increases in PNO_3 in China were dominated by an upward trend in O_3 rather than NO_2 (Fig. 1d). The reduction of nocturnal NO_x emission led to a rapid increase of nocturnal O_3 (6.3%) in the four regions. In addition, we observed nocturnal surface temperature has an increasing tendency (0.06%) in this period that contributed to the rise in PNO_3 via $k_{\text{NO}_2+\text{O}_3}$ by 0.53%, showing that nocturnal chemical processes are modestly affected by global climate change²⁰. The decrease in NO_2 offset the effect of O_3 increase to PNO_3 changes in three megacities (North China Plain, Yangtze River Delta and Pearl River Delta) and was significant in the North China Plain. NO_2 increased only in Sichuan Basin, which made a considerable contribution to PNO_3 . Similar distributions and trends also occurred in the cold season (Extended Data Figs. 3 and 4), suggesting that the hotspot of NO_3 chemistry persisted for the entire year in China.

We also calculated PNO_3 in late afternoon (16:00–19:00 LT), which is a proxy for PNO_3 in the residual layer to some extent²¹ since late-afternoon surface measurements in a well-mixed boundary layer may in some cases be characteristic of the initial composition of the residual layer after dark. However, we acknowledge that this property of the afternoon boundary layer is not universal and depends on the nature of the site (for example, coastal versus continental) and season. Late-afternoon PNO_3 showed a similar distribution globally and an upward trend in China, highlighting that strong NO_3 oxidation occurs in both the nocturnal boundary layer and the residual layer (Supplementary Figs. 2 and 3).

Atmospheric impacts of PNO_3 change

Assuming the fate of produced NO_3 is to convert organic or inorganic nitrate, leading to removal of NO_x , we show the intensive and accelerated night-time oxidation shortened the nocturnal surface NO_x lifetime (τ_{NO_2}) by $\sim 30\%$ from a median of 10.2 h in 2014 to 7.3 h in 2019 (Methods) in the warm season in China and shortened the residual-layer τ_{NO_2} from 4.1 h to 3.1 h, while it was stabilized at high level in other regions in this period (Extended Data Fig. 5 and Supplementary Table 1). The nocturnal surface τ_{NO_2} in China is comparable to the daytime τ_{NO_2} in some urban regions^{22,23}, while the residual-layer τ_{NO_2} is comparable to or faster than that of photochemical oxidation over a range of conditions. Reduction of the nocturnal τ_{NO_2} is important since the nocturnal contribution to oxidation of NO_x varies from $\sim 30\%$ of the total in summer to as much as 90% in the winter^{24–27}. The reduction in τ_{NO_2} changes the amount of NO_x available for photochemistry at sunrise and the formation of night-time nitrate aerosols, demonstrating the growing importance of nocturnal oxidation processes in China. For example, an integrated 10 h PNO_3 of 1 ppbv hr^{-1} would be equivalent to a maximum of approximately $50 \mu\text{g m}^{-3}$ nitrate aerosol at unit yield. Since eastern China is characterized by intensive biogenic emissions²⁸, anthropogenic monoterpene emission²⁹ and higher values of PNO_3 , more NO_3 is produced there, which accelerates the oxidation of VOC and has the potential to enhance organic aerosol pollution. For example, if a molecular weight of an oxidation product (monoterpene nitrate) were 250 g mol^{-1} with a yield of 30% (ref. 3), this would suggest $25 \mu\text{g m}^{-3}$ potential overnight (10 h) SOA formation if the limiting reagent were the VOC. In addition, the activation of chlorine atoms through the production of ClNO_2 via increased N_2O_5 uptake promotes photochemical pollution^{30,31} if the ClNO_2 yield does not change. Given that the much lower values of PNO_3 in both the European Union and the United States have been shown to exert significant impacts on the particulate nitrate and organic aerosol formation in those regions^{3–5,32}, we infer that NO_3 chemistry may play a more critical role in atmospheric oxidation and aggravate both O_3 and $\text{PM}_{2.5}$ pollution in China.

Considering the short lifetime of NO_3 in the atmosphere, trends in the loss of NO_3 are also important but are probably separate from those in PNO_3 . Unlike the single dominant source of NO_3 , its loss is much more complicated, governed by the reaction of NO_3 with VOCs and the uptake of N_2O_5 . In terms of the reaction between NO_3 and

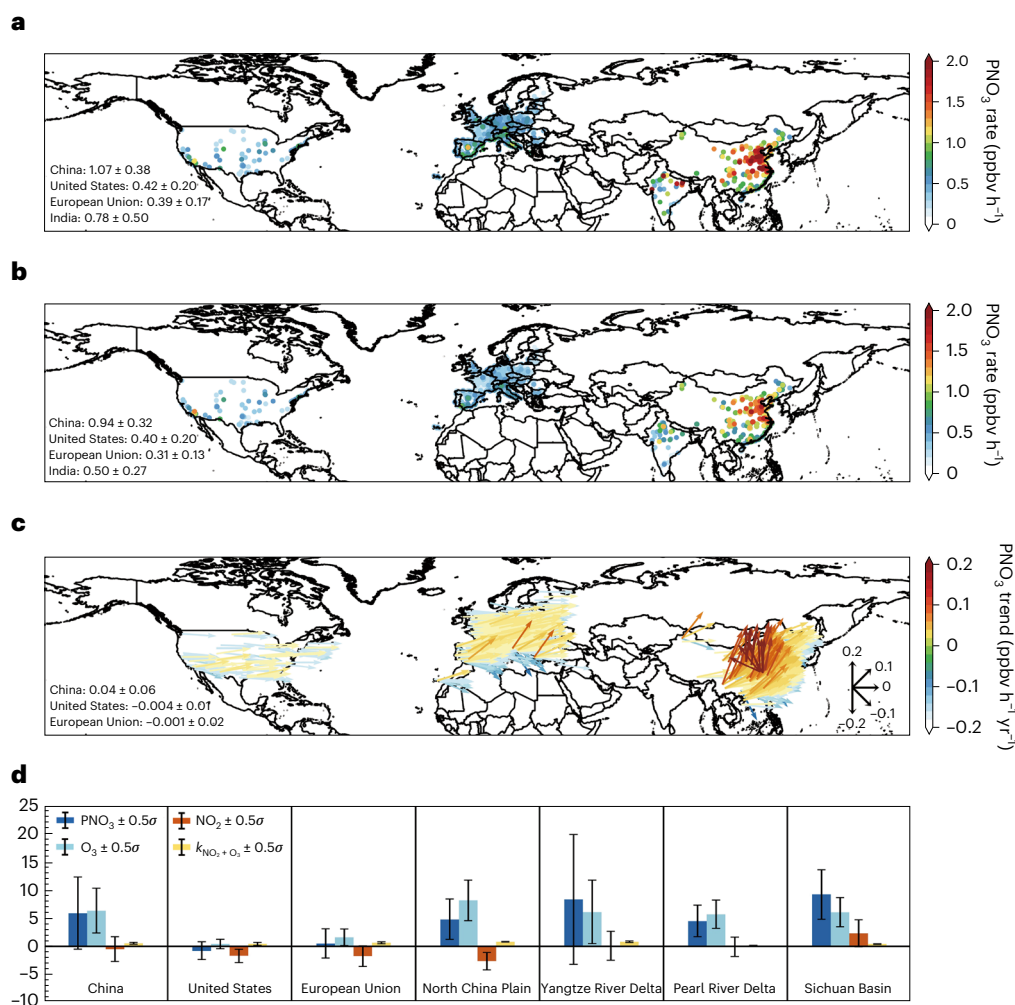


Fig. 1 | Observed level and trend of nocturnal PNO_3 in the warm season.

a–c, Warm-season average nocturnal PNO_3 for 2018–2019 (**a**) and 2020–2021 (**b**) and the nocturnal PNO_3 trend for 2014–2019 (**c**) in the United States, the European Union, India and China. Both direction and colour of the vectors indicate the change rates of PNO_3 in $\text{ppbv h}^{-1} \text{yr}^{-1}$. **d**, The change of PNO_3 ,

night-time O_3 and NO_2 and its reaction rate ($k_{\text{NO}_2 + \text{O}_3}$) in percentage (mean $\pm 50\%$ standard deviation, 0.5σ) in the United States, the European Union, China and four Chinese city clusters (North China Plain, Yangtze River Delta, Pearl River Delta and Sichuan Basin) during 2014–2019. Basemap reproduced from ref.⁵² under a Creative Commons license CC BY 4.0.

VOCs, the major NO_3 reactants are biogenic terpenes at the global scale. Such biogenic emissions are influenced mainly by temperature and should not change much in terms of long-term trends during the six years analysed here. In the urban and city clusters scale, anthropogenic VOC emissions may be significant in the early period in areas such as Los Angeles and have been decreasing with the continuous implementation of emission reductions. Therefore, it can be assumed that the NO_3 reactivity contributed by anthropogenic VOC has decreased substantially in Los Angeles. In China, by contrast, VOC emissions showed a small increase in recent years (2010–2017)³³; thus, an increase in anthropogenic NO_3 reactivity can be expected. In terms of the N_2O_5 uptake, the sharp decrease in aerosol loading in China during 2014–2019³⁴ led to a decreasing surface area for the reaction taking place. At the same time, the decrease in sulfate and the increase in nitrate fraction potentially further reduce the N_2O_5 uptake rate. Long-term decreases in aerosol in the United States are well documented^{35–37} but have not been analysed in terms of the influence on N_2O_5 uptake. Above all, the NO_3 loss frequency may show some decline (considering the increased anthropogenic VOC enhanced little NO_3 reactivity) in China and be stable or decrease slightly in the European Union and the United States. This implies an increasing trend in NO_3 concentration in China.

This increasing trend was interrupted by the COVID-19 pandemic. Figure 1b shows that PNO_3 decreased by 10–40% in different regions during 2020–2021 compared with 2018–2019, which is attributed to the consistent global decline in concentrations of both nocturnal NO_2 and O_3 (Extended Data Fig. 1c,d). However, the dramatic emission change initiated by the pandemic does not appear to have been sustained³⁸. Emissions and pollution conditions have largely rebounded to pre-pandemic levels in the United States and the European Union and will probably do so in China in the future³⁹. Thus, atmospheric chemical cycles initiated by night-time chemistry are likely to return to pre-pandemic rates.

Air pollution control strategies from night-time chemical perspective

We further constructed a theoretical framework (Methods) to describe the dependence of PNO_3 on NO_x emissions at different levels of VOCs (Fig. 3a). Under a fixed VOC emission scenario, a decrease in NO_x from a high emission level weakens NO titration of O_3 and increases PNO_3 . We term this the NO_x -saturated regime for night-time chemistry, analogous to the similarly named photochemical regime⁴⁰. At much lower NO_x emissions, the decrease in NO_x reduces O_3 formation during the previous day and leads to proportional decline of PNO_3 at night.

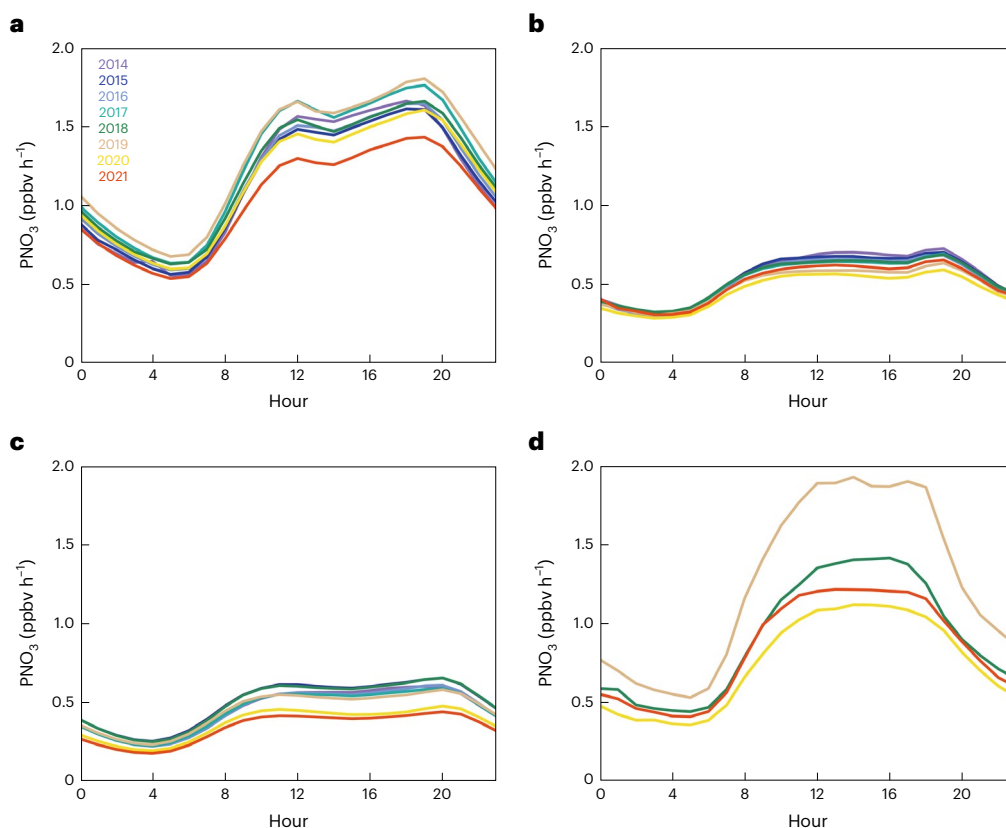


Fig. 2 | The annual mean diurnal cycle of PNO₃ by region. a–d, Annual mean diurnal cycle of PNO₃ for 2014–2021 in China (a), the United States (b) and the European Union (c) and for 2018–2022 in India (d).

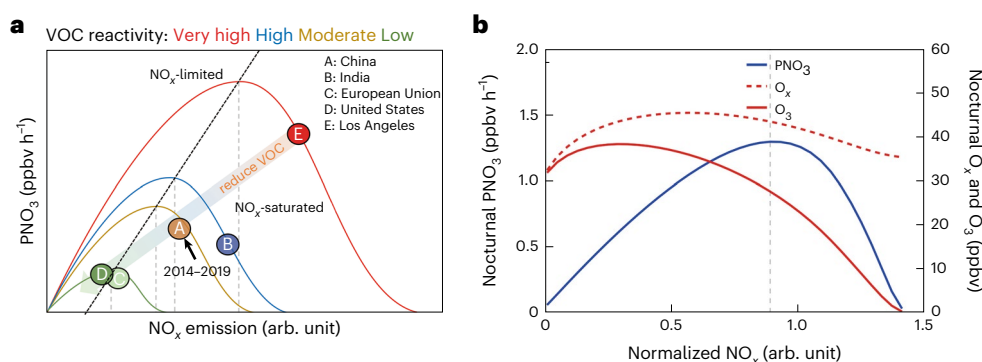


Fig. 3 | Conceptual framework on the dependence of PNO₃ on NO_x emission. a, Dependence of PNO₃ on NO_x emission in China, India, the European Union and the United States during 2018–2019 and Los Angeles in 1980. The colour of the curve represents the dependence at different VOC reactivity. The black dotted line is the dividing line between the NO_x-limited regime and the NO_x-saturated

regime. The coloured arrow indicates the experience of Los Angeles since 1980, and the black arrow indicates the trend of China cities during 2014–2019. The location was adapted from the Extended Data Fig. 6. **b**, The dependence of average nocturnal PNO₃ on NO_x emission with a fixed VOC emission. The dotted line denotes the maximum of PNO₃.

We term this the NO_x-limited night-time regime. The evolution of these two patterns is attributed to the nonlinear relationship between O₃ and its precursors. Specifically, PNO₃ is regulated by total oxidants (O_x = NO₂ + O₃) and their nocturnal distribution (Fig. 3b). Both aspects are affected by NO_x emission, and the maximum nocturnal PNO₃ would occur under conditions in which nocturnal NO₂ is approximately equal to O₃.

We found Chinese and Indian cities located in the NO_x-saturated regime; the European Union and the United States are currently transitioning to the NO_x-limited regime, where the change in PNO₃ with

NO_x reduction is weak. Historical long-term records show that Los Angeles experienced an overall persistent decrease in PNO₃ with a continuous reduction of NO₂ and stabilized nocturnal O₃ levels in the past four decades. Ref. ⁴¹ reported the first measurements of urban NO₃ during 15 nights in August–September 1979 at Claremont and Riverside in the Los Angeles Basin. Analysis of their reported NO₂, O₃ and temperature at the time of the NO₃ maximum, which occurred at or just after sunset, indicated PNO₃ of 13.2 ± 13.2 ppbv h⁻¹, with a maximum value of 52.7 ppbv h⁻¹. A single 6 h event from 18:00–midnight LT on 18 September 1979 showed PNO₃ = 30.9 ± 18.6 ppbv h⁻¹, with a maximum

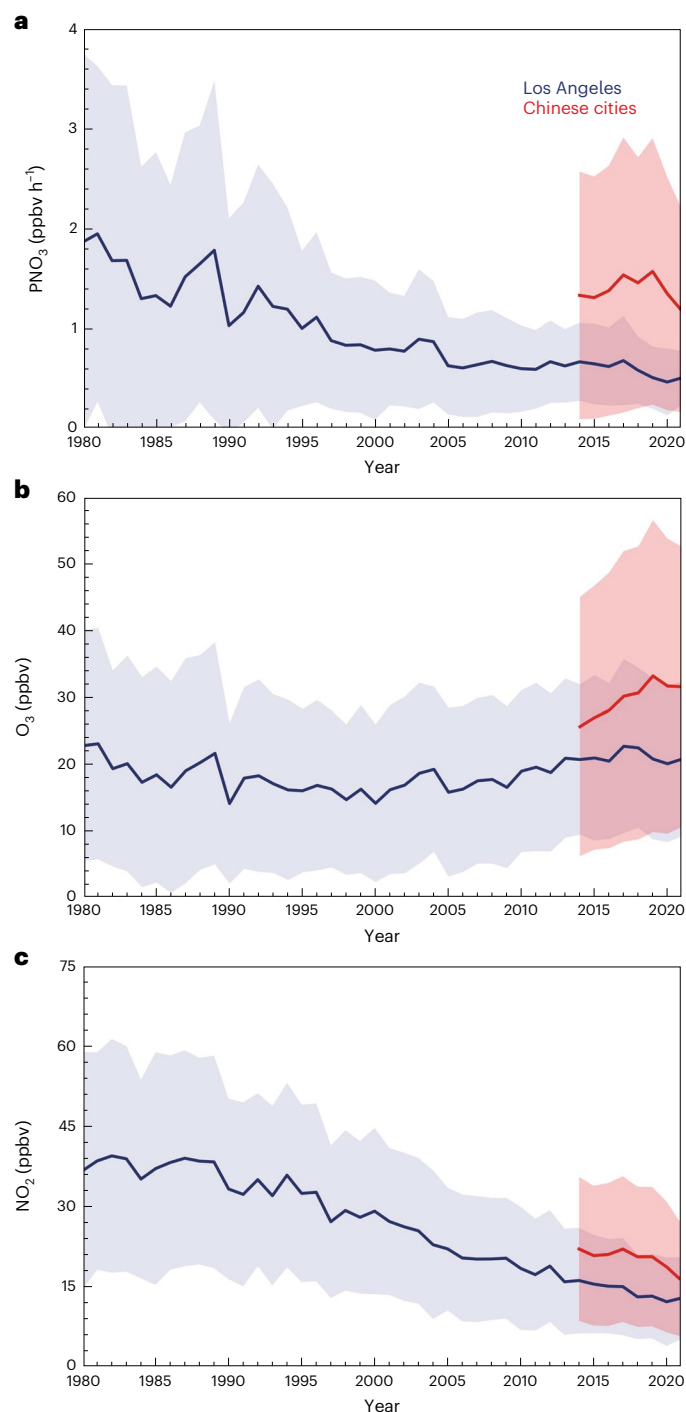


Fig. 4 | The warm-season trends of nocturnal PNO₃, NO₂ and O₃ from 1980 to 2021. **a–c.** The annual trend (mean ± standard deviation) of nocturnal PNO₃ (**a**), O₃ (**b**) and NO₂ (**c**) in Los Angeles and eight representative Chinese cities (Beijing, Shanghai, Guangzhou, Chengdu, Xi'an, Jinan, Zhengzhou and Shijiazhuang) in the warm season from 1980 to 2021. The results in the cold season are shown in Extended Data Fig. 7.

of 65.8 ppbv h⁻¹. Thus, much larger values of PNO₃ during extreme air pollution events occurred in Los Angeles during this time.

The current PNO₃ diagnosed in eight representative cities (Beijing, Shanghai, Guangzhou, Chengdu, Xi'an, Jinan, Zhengzhou and Shijiazhuang) in China is comparable to that in 1990s Los Angeles, but with an overall increasing trend during 2014–2019 accompanied by NO_x decrease (Fig. 4). This is because O₃ formation in many Chinese

cities is under the VOC-limited regime, such that the reduction of NO_x would increase O₃ (ref. 42). The long-term decreasing trend in PNO₃ in Los Angeles illustrates that the level of nocturnal O₃ can be stabilized while reducing NO_x simultaneously, a result that may also apply in China. Combining the theoretical framework and the observed shift during the COVID-19 pandemic³⁸, we propose that the night-time oxidation rate is closely affected by daytime O₃ pollution. Reduction in VOCs is therefore an effective mitigation strategy for both daytime O₃ pollution and night-time NO₂-initiated chemical cycles in China and similar developing countries such as India⁴³, unless a shift occurs to the NO_x-limited regime.

The decreased NO_x lifetime and increased night-time oxidation have the potential to significantly impact air quality. The recent trend in Chinese cities shows a counterintuitive increase of PNO₃ with NO_x reduction, implying that night-time chemistry will become increasingly more important due to the continued future PNO₃ increase in China. This increase has the potential to further increase rates of important cycles influencing air quality such as nitrate aerosol and SOA production^{2,44} and halogen cycling, which influences O₃ pollution^{12,13}. These results demonstrate the challenge in mitigating photochemical and nitrate aerosol pollution related to nocturnal oxidation in the urban agglomeration of China^{43,45,46}, and likewise in developing countries such as India⁴⁷. Therefore, elucidating the mechanisms and developing cost-effective mitigation strategies for night-time oxidation changes will be critical for understanding the evolution of the tropospheric oxidation capacity^{48–51} and its role in air quality and climate. Only a limited number of modelling studies quantitatively assess the response of O₃ and PM to night-time chemical processes, let alone to trends in the initiation of these processes. Explicit consideration of such trends in future modelling studies will be of substantial interest to assessment of air quality and climate responses to emissions changes.

Online content

Any methods, additional references, Nature Portfolio reporting summaries, source data, extended data, supplementary information, acknowledgements, peer review information; details of author contributions and competing interests; and statements of data and code availability are available at <https://doi.org/10.1038/s41561-022-01122-x>.

References

1. Brown, S. S. & Stutz, J. Nighttime radical observations and chemistry. *Chem. Soc. Rev.* **41**, 6405–6447 (2012).
2. Ng, N. L. et al. Nitrate radicals and biogenic volatile organic compounds: oxidation, mechanisms, and organic aerosol. *Atmos. Chem. Phys.* **17**, 2103–2162 (2017).
3. Kiendler-Scharr, A. et al. Ubiquity of organic nitrates from nighttime chemistry in the European submicron aerosol. *Geophys. Res. Lett.* **43**, 7735–7744 (2016).
4. Zhang, H. F. et al. Monoterpenes are the largest source of summertime organic aerosol in the southeastern United States. *Proc. Natl Acad. Sci. USA* **115**, 2038–2043 (2018).
5. Rollins, A. W. et al. Evidence for NO_x control over nighttime SOA formation. *Science* **337**, 1210–1212 (2012).
6. Pye, H. O. T., Chan, A. W. H., Barkley, M. P. & Seinfeld, J. H. Global modeling of organic aerosol: the importance of reactive nitrogen (NO_x and NO₂). *Atmos. Chem. Phys.* **10**, 11261–11276 (2010).
7. Hoyle, C. R., Berntsen, T., Myhre, G. & Isaksen, I. S. A. Secondary organic aerosol in the global aerosol–chemical transport model Oslo CTM2. *Atmos. Chem. Phys.* **7**, 5675–5694 (2007).
8. Hoyle, C. R., Myhre, G., Berntsen, T. K. & Isaksen, I. S. A. Anthropogenic influence on SOA and the resulting radiative forcing. *Atmos. Chem. Phys.* **9**, 2715–2728 (2009).
9. Hoyle, C. R. et al. A review of the anthropogenic influence on biogenic secondary organic aerosol. *Atmos. Chem. Phys.* **11**, 321–343 (2011).

10. Wang, H. et al. High N₂O₅ concentrations observed in urban Beijing: implications of a large nitrate formation pathway. *Environ. Sci. Technol. Lett.* **4**, 416–420 (2017).
11. Wang, M. Y. et al. Rapid growth of new atmospheric particles by nitric acid and ammonia condensation. *Nature* **581**, 184–189 (2020).
12. Osthoff, H. D. et al. High levels of nitryl chloride in the polluted subtropical marine boundary layer. *Nat. Geosci.* **1**, 324–328 (2008).
13. Thornton, J. A. et al. A large atomic chlorine source inferred from mid-continental reactive nitrogen chemistry. *Nature* **464**, 271–274 (2010).
14. Macintyre, H. L. & Evans, M. J. Sensitivity of a global model to the uptake of N₂O₅ by tropospheric aerosol. *Atmos. Chem. Phys.* **10**, 7409–7414 (2010).
15. Sarwar, G., Simon, H., Xing, J. & Mathur, R. Importance of tropospheric ClNO₂ chemistry across the Northern Hemisphere. *Geophys. Res. Lett.* **41**, 4050–4058 (2014).
16. Li, K. et al. Ozone pollution in the North China Plain spreading into the late-winter haze season. *Proc. Natl Acad. Sci. USA* <https://doi.org/10.1073/pnas.2015797118> (2021).
17. Fleming, Z. L. et al. Tropospheric Ozone Assessment Report: present-day ozone distribution and trends relevant to human health. *Elementa* <https://doi.org/10.1525/elementa.273> (2018).
18. Wang, H. et al. Characterizing nitrate radical budget trends in Beijing during 2013–2019. *Sci. Total Environ.* <https://doi.org/10.1016/j.scitotenv.2021.148869> (2021).
19. Lu, X. et al. Rapid increases in warm-season surface ozone and resulting health impact in China since 2013. *Environ. Sci. Technol. Lett.* <https://doi.org/10.1021/acs.estlett.0c00171> (2020).
20. Sharifnezhadazizi, Z., Norouzi, H., Prakash, S., Beale, C. & Khanbilvardi, R. A global analysis of land surface temperature diurnal cycle using MODIS observations. *J. Appl Meteorol. Clim.* **58**, 1279–1291 (2019).
21. Baasandorj, M. et al. Coupling between chemical and meteorological processes under persistent cold-air pool conditions: evolution of wintertime PM_{2.5} pollution events and N₂O₅ observations in Utah's Salt Lake Valley. *Environ. Sci. Technol.* **51**, 5941–5950 (2017).
22. Beirle, S., Boersma, K. F., Platt, U., Lawrence, M. G. & Wagner, T. Megacity emissions and lifetimes of nitrogen oxides probed from space. *Science* **333**, 1737–1739 (2011).
23. Laughner, J. L. & Cohen, R. C. Direct observation of changing NO_x lifetime in North American cities. *Science* **366**, 723–727 (2019).
24. Brown, S. S. et al. Nighttime removal of NO_x in the summer marine boundary layer. *Geophys. Res. Lett.* <https://doi.org/10.1029/2004gl019412> (2004).
25. Kenagy, H. S. et al. NO_x lifetime and NO_y partitioning during WINTER. *J. Geophys. Res. Atmos.* **123**, 9813–9827 (2018).
26. McDuffie, E. E. et al. On the contribution of nocturnal heterogeneous reactive nitrogen chemistry to particulate matter formation during wintertime pollution events in Northern Utah. *Atmos. Chem. Phys.* **19**, 9287–9308 (2019).
27. Womack, C. C. et al. An odd oxygen framework for wintertime ammonium nitrate aerosol pollution in urban areas: NO_x and VOC control as mitigation strategies. *Geophys. Res. Lett.* **46**, 4971–4979 (2019).
28. Sindelarova, K. et al. Global data set of biogenic VOC emissions calculated by the MEGAN model over the last 30 years. *Atmos. Chem. Phys.* **14**, 9317–9341 (2014).
29. Wang, H. et al. Anthropogenic monoterpenes aggravating ozone pollution. *Natl Sci. Rev.* <https://doi.org/10.1093/nsr/nwac103> (2022).
30. Wang, T. et al. Observations of nitryl chloride and modeling its source and effect on ozone in the planetary boundary layer of southern China. *J. Geophys. Res. Atmos.* **121**, 2476–2489 (2016).
31. Peng, X. et al. Photodissociation of particulate nitrate as a source of daytime tropospheric Cl₂. *Nat. Commun.* <https://doi.org/10.1038/s41467-022-28383-9> (2022).
32. Franchin, A. et al. Airborne and ground-based observations of ammonium-nitrate-dominated aerosols in a shallow boundary layer during intense winter pollution episodes in northern Utah. *Atmos. Chem. Phys.* **18**, 17259–17276 (2018).
33. Zheng, B. et al. Trends in China's anthropogenic emissions since 2010 as the consequence of clean air actions. *Atmos. Chem. Phys.* **18**, 14095–14111 (2018).
34. Wang, Y. H. et al. Contrasting trends of PM_{2.5} and surface-ozone concentrations in China from 2013 to 2017. *Natl Sci. Rev.* **7**, 1331–1339 (2020).
35. Attwood, A. R. et al. Trends in sulfate and organic aerosol mass in the southeast US: impact on aerosol optical depth and radiative forcing. *Geophys. Res. Lett.* **41**, 7701–7709 (2014).
36. Blanchard, C. L., Hidy, G. M., Shaw, S., Baumann, K. & Edgerton, E. S. Effects of emission reductions on organic aerosol in the southeastern United States. *Atmos. Chem. Phys.* **16**, 215–238 (2016).
37. Hand, J. L., Prenni, A. J., Copeland, S., Schichtel, B. A. & Malm, W. C. Thirty years of the Clean Air Act Amendments: impacts on haze in remote regions of the United States (1990–2018). *Atmos. Environ.* <https://doi.org/10.1016/j.atmosenv.2020.117865> (2020).
38. Shi, Z. B. et al. Abrupt but smaller than expected changes in surface air quality attributable to COVID-19 lockdowns. *Sci. Adv.* <https://doi.org/10.1126/sciadv.abd6696> (2021).
39. Liu, Q. et al. Spatiotemporal changes in global nitrogen dioxide emission due to COVID-19 mitigation policies. *Sci. Total Environ.* <https://doi.org/10.1016/j.scitotenv.2021.146027> (2021).
40. Seinfeld, J. H. Urban air pollution: state of the science. *Science* **243**, 745–752 (1989).
41. Platt, U., Perner, D., Winer, A. M., Harris, G. W. & Pitts, J. N. Jr. Detection of NO₃ in the polluted troposphere by differential optical absorption. *Geophys. Res. Lett.* **7**, 89–92 (1980).
42. Tan, Z. et al. Explicit diagnosis of the local ozone production rate and the ozone–NO_x–VOC sensitivities. *Sci. Bull.* **63**, 1067–1076 (2018).
43. Li, K. et al. A two-pollutant strategy for improving ozone and particulate air quality in China. *Nat. Geosci.* **12**, 906–910 (2019).
44. Ehn, M. et al. A large source of low-volatility secondary organic aerosol. *Nature* **506**, 476–479 (2014).
45. Zhai, S. et al. Control of particulate nitrate air pollution in China. *Nat. Geosci.* **14**, 389–395 (2021).
46. Nie, W. et al. Secondary organic aerosol formed by condensing anthropogenic vapours over China's megacities. *Nat. Geosci.* **15**, 255–261 (2022).
47. Meidan, D., Brown, S. S., Sinha, V. & Rudich, Y. Nocturnal atmospheric oxidative processes in the Indo-Gangetic plain and their variation during the COVID-19 lockdowns. *Geophys. Res. Lett.* **49**, e2021GL097472 (2022).
48. Lu, X. et al. Severe surface ozone pollution in China: a global perspective. *Environ. Sci. Technol. Lett.* **5**, 487–494 (2018).
49. Gaudel, A. et al. Aircraft observations since the 1990s reveal increases of tropospheric ozone at multiple locations across the Northern Hemisphere. *Sci. Adv.* <https://doi.org/10.1126/sciadv.aba8272> (2020).
50. Murray, L. T., Fiore, A. M., Shindell, D. T., Naik, V. & Horowitz, L. W. Large uncertainties in global hydroxyl projections tied to fate of reactive nitrogen and carbon. *Proc. Natl Acad. Sci. USA* <https://doi.org/10.1073/pnas.2115204118> (2021).
51. Zhu, Q. D., Laughner, J. L. & Cohen, R. C. Estimate of OH trends over one decade in North American cities. *Proc. Natl Acad. Sci. USA* <https://doi.org/10.1073/pnas.2117399119> (2022).

52. Wang, H. L. et al. Global tropospheric ozone trends, attributions, and radiative impacts in 1995–2017: an integrated analysis using aircraft (IAGOS) observations, ozonesonde, and multi-decadal chemical model simulations. *Atmos. Chem. Phys.* **22**, 13753–13782 (2022).

Publisher's note Springer Nature remains neutral with regard to jurisdictional claims in published maps and institutional affiliations.

Springer Nature or its licensor (e.g. a society or other partner) holds exclusive rights to this article under a publishing agreement with the author(s) or other rightsholder(s); author self-archiving of the accepted manuscript version of this article is solely governed by the terms of such publishing agreement and applicable law.

© The Author(s), under exclusive licence to Springer Nature Limited 2023

Methods

Observation and reanalysis data

The nationwide hourly observations of ground-level NO₂ and O₃ at more than 1,600 stations in Chinese cities for 2014–2021 were obtained from the China National Environmental Monitoring Center network. Concurrent hourly measurements in the United States (including Los Angeles for 1980–2021) and the European Union were obtained from the Environmental Protection Agency Air Quality System monitoring network and the European Environment Agency, respectively. Ground observations of NO₂ and O₃ monitored at the Central Pollution Control Board continuous stations in India are available from the Central Control Room for Air Quality Management for 2014–2021. Hourly air temperature at 2 m above the ground (T2M) was obtained from the NASA (National Aeronautics and Space Administration) Modern-Era Retrospective Analysis for Research and Applications, version 2 (MERRA-2) product⁵³ at a resolution of 0.5° × 0.625°. We sample MERRA-2 temperature data at the grid of a monitoring site to calculate the NO₃ production rate for individual sites.

Data quality control

The measurements of NO₂ and O₃ are converted to mixing ratio (ppbv) at local time. We apply data quality-control measures to exclude unreliable data outliers and select stations with continuous observations from 2014 to 2021 for trend analysis. Following previous studies^{19,54,52}, we exclude data points (1) with values greater than 500 ppbv or less than 0 ppbv, (2) with an hourly standardized value ($z_i = \frac{x_i - \bar{x}}{\sigma}$, where x_i is the hourly data point, \bar{x} is the monthly mean value and σ is the standard deviation calculated for each month) larger than 5, (3) showing extremely low variability in a specific day (the difference between the daily maximum and minimum is less than 2 ppbv), (4) with the same value for at least 4 of 5 consecutive hours or (5) showing unrealistic huge spikes in time series that meet the criteria of ref. ¹⁹. These quality-control procedures removed 4.4%, 12.3%, 12.4% and 13.3% of the hourly records in China, the United States, the European Union and India, respectively. Some of the NO₂ monitoring network data used in this study are based on conversion to NO using a heated molybdenum catalyst, a method known to have positive interferences that increase with the ratio of oxidized reactive nitrogen to NO_x (refs. ^{55,56}). This effect makes the determined PNO₃ from this work an upper limit to the actual PNO₃, except in networks that use photolytic converters or direct NO₂ monitors (for example, the US state of California) or in source regions where NO_x is a large fraction of total reactive nitrogen.

The calculation of nocturnal NO_x lifetime

The nocturnal NO_x lifetime (τ_{NO_x}) is calculated by equation (2). Here, we estimated the lower limit of nocturnal NO_x lifetime assuming NO₃ loss is dominated by N₂O₅ uptake; therefore, the loss of NO₃ is accompanied by an additional NO₂ loss:

$$\tau_{\text{NO}_x} = [\text{NO}_2] / (2 \times \text{PNO}_3) = 1 / (2 \times k_{\text{NO}_2+\text{O}_3} [\text{O}_3]) \quad (2)$$

Nocturnal nitrate production rate and trend analysis

Nocturnal nitrate production rate is the average of hourly NO₃ production rate for the 10 h period from 20:00 to 05:59 (the next day) LT. At least 75% (7 h) of valid hourly records are required to calculate the daily nocturnal average value. The valid daily records availability requirement was relaxed to 60% (18 d) to calculate the monthly mean value. Monthly mean values of nocturnal NO₃ production rate are then used to determine their trends at each site. We use only sites with at least 60% (21 months) of available monthly records in 2014–2019 and at least four valid monthly records in 2014 to derive the trends. Therefore, 506 sites in China, 116 sites in the United States and 1,004 sites in the European Union are used to calculate the trends in nocturnal NO₃ production rate in the warm (April–September) and cold (other months) seasons.

For India, we calculate the mean nocturnal NO₃ production rate at 49 sites for 2018–2019 and at 78 sites for 2020–2021 since the data for 2014–2017 are largely unavailable and do not meet the preceding requirements for trend calculation. In addition, as both NO₂ and O₃ have strong seasonal cycles, trends in nocturnal PNO₃ based on monthly averages can be less accurate than trends derived from monthly anomalies, if there are missing data⁵⁷. We thus follow the strategy proposed by Cooper et al.⁵⁷ to calculate trends on the basis of monthly average anomalies. We first calculate monthly averages for the entire period 2014–2019 and then yield the monthly anomaly value as the difference between individual monthly mean and the 2014–2019 monthly mean values. The linear trends in NO₃ production rates are estimated using the following generalized least-squares method with autoregression¹⁹:

$$y_t = b + kt + \alpha \cos\left(\frac{2\pi M}{6}\right) + \beta \sin\left(\frac{2\pi M}{6}\right) + \text{AR}_t \quad (3)$$

where y_t represents the monthly nocturnal NO₃ production rate anomaly in month t , t is the index of month during the study period (warm/cold season for 2014–2019, that is, ranging from 1 to 36), b is the intercept, k denotes the linear trend coefficient, α and β are coefficients for a 6 month harmonic series of seasonal cycle (M ranges from 1 to 6) and AR_t is to account for autocorrelation.

The set-up of framework for sensitivity test of PNO₃ and NO₂

An observationally constrained box model based on the Regional Atmospheric Chemical Mechanism version 2 (RACM2)⁵⁸, with some modifications (such as the chloride chemistry was added⁵⁹) is applied in this study. A detailed description of the implementation of RACM2 can be found in a previous publication⁵⁹. In this study, the model calculations are constrained to measurements of CO, SO₂, C₂–C₁₂ VOC as well as the measured photolysis frequencies, temperature and pressure, and water-vapour concentrations and aerosol surface-area density. NO_x emission rate, retrieved by fitting the observed diurnal NO_x and O₃ concentrations, was also constrained. The CH₄ and H₂ mixing ratios are assumed to be 1.9 ppmv and 550 ppbv, respectively. The model is operated in a time-dependent mode, in which constrained values are updated every 1 h. For all species that are produced in the model, an additional sink representing physical loss processes such as dry deposition is implemented at a rate equivalent to a lifetime of 24 h. The heterogeneous chemistries of N₂O₅ and ClNO₂ were considered in the box model. The N₂O₅ uptake coefficient was adopted by the parameterization scheme considering the ambient temperature and relative humidity⁶⁰, with a fixed ClNO₂ yield of 0.5. The ClNO₂ uptake coefficient was adopted by an upper value of 5×10^{-6} with a unit Cl₂ yield^{61,62}.

The dependence of PNO₃ on the NO_x emission is calculated using the box model. The chemical mechanisms are the same as described in the preceding. Therefore, the model is prescribed to different NO_x emission rates, which is more representative of the real-world conditions. We used the diurnal average observation data, obtained in Taizhou in east China during summer 2018⁶³, as a base-case constraint with an additional 2 d spin-up. By adjusting the intensity of NO_x emission along with the constrained VOC reactivity, the modelled NO₂ and O₃ are optimized to match the observations, and then we subsequently derived the NO_x emission in the base case. By adjusting the factor of NO_x emission and VOC reactivity, we can then enable the conceptual model to fit the observationally derived PNO₃, O₃ and NO_x for the average condition of China, the United States, the European Union and India during 2018–2019 and the case in Los Angeles in 1980 (Extended Data Fig. 6). We checked the influences of aerosol loading, solar radiation and surface temperature on the pattern of PNO₃–NO_x emission by sensitivity tests and confirmed that these factors did not change the pattern of the curve and relative positions of different cities but led to some squeeze and shift in the peak of the curve as well as its width.

Data availability

The data are available via figshare (<https://doi.org/10.6084/m9.figshare.20290587.v4>). The hourly ground-based observations of NO₂ and O₃ over China, the United States, the European Union and India are archived at <https://quotsoft.net/air/>, <https://www.epa.gov/outdoor-air-quality-data>, <https://discomap.eea.europa.eu/map/fme/AirQualityExport.htm> and <https://app.cpcbcr.com/ccr/>, respectively. The hourly 2 m air temperature MERRA-2 reanalysis data are from <https://doi.org/10.5067/VJAFPLIICSIV>. The box-model simulation dataset is available via figshare (<https://doi.org/10.6084/m9.figshare.21268014>). Source data are provided with this paper.

Code availability

All figures in this article are produced by the IDL (Interactive Data Language version 8.3) and python, and the source codes can be obtained upon request to the corresponding authors.

References

- Gelaro, R. et al. The Modern-Era Retrospective Analysis for Research and Applications, Version 2 (MERRA-2). *J. Clim.* **30**, 5419–5454 (2017).
- Jiang, Z. et al. Impact of western Pacific subtropical high on ozone pollution over eastern China. *Atmos. Chem. Phys.* **21**, 2601–2613 (2021).
- Demerjian, K. L. A review of national monitoring networks in North America. *Atmos. Environ.* **34**, 1861–1884 (2000).
- Dunlea, E. J. et al. Evaluation of nitrogen dioxide chemiluminescence monitors in a polluted urban environment. *Atmos. Chem. Phys.* **7**, 2691–2704 (2007).
- Cooper, O. R. et al. Multi-decadal surface ozone trends at globally distributed remote locations. *Elementa* <https://doi.org/10.1525/elementa.420> (2020).
- Goliff, W. S., Stockwell, W. R. & Lawson, C. V. The Regional Atmospheric Chemistry Mechanism, version 2. *Atmos. Environ.* **68**, 174–185 (2013).
- Tan, Z. et al. Radical chemistry at a rural site (Wangdu) in the North China Plain: observation and model calculations of OH, HO₂ and RO₂ radicals. *Atmos. Chem. Phys.* **17**, 663–690 (2017).
- Evans, M. J. & Jacob, D. J. Impact of new laboratory studies of N₂O₅ hydrolysis on global model budgets of tropospheric nitrogen oxides, ozone, and OH. *Geophys. Res. Lett.* <https://doi.org/10.1029/2005gl022469> (2005).
- Roberts, J. M., Osthoff, H. D., Brown, S. S. & Ravishankara, A. R. N₂O₅ oxidizes chloride to Cl₂ in acidic atmospheric aerosol. *Science* **321**, 1059–1059 (2008).
- Roberts, J. M. et al. Laboratory studies of products of N₂O₅ uptake on Cl-containing substrates. *Geophys. Res. Lett.* <https://doi.org/10.1029/2009gl040448> (2009).
- Wang, H. et al. NO₃ and N₂O₅ chemistry at a suburban site during the EXPLORE-YRD campaign in 2018. *Atmos. Environ.* <https://doi.org/10.1016/j.atmosenv.2019.117180> (2020).

Acknowledgements

Haichao Wang received financial support from the National Natural Science Foundation of China (grant 42175111). K.L. received financial support from the National Natural Science Foundation of China (grants 22221004, 21976006, 91844301). K.L. received financial support from the Beijing Municipal Natural Science Foundation for Distinguished Young Scholars (JQ19031). K.L. received financial support from the National Research Program for Key Issue in Air Pollution Control (2019YFC0214800). Haichao Wang received financial support from the National State Environmental Protection Key Laboratory of Formation and Prevention of Urban Air Pollution Complex (grant CX2020080578). Y.J.T. received financial support from National Natural Science Foundation of China (42175118) and Guangdong Basic and Applied Basic Research Foundation (2022A1515010852).

Author contributions

Haichao Wang, K.L., S.S.B. and Y.Z. designed the study. Haichao Wang, K.L., Haolin Wang, K.A. and X.L. analysed the data and wrote the paper with input from L.Z., Y.J.T., Z.S. and S.F.

Competing interests

The authors declare no competing interests.

Additional information

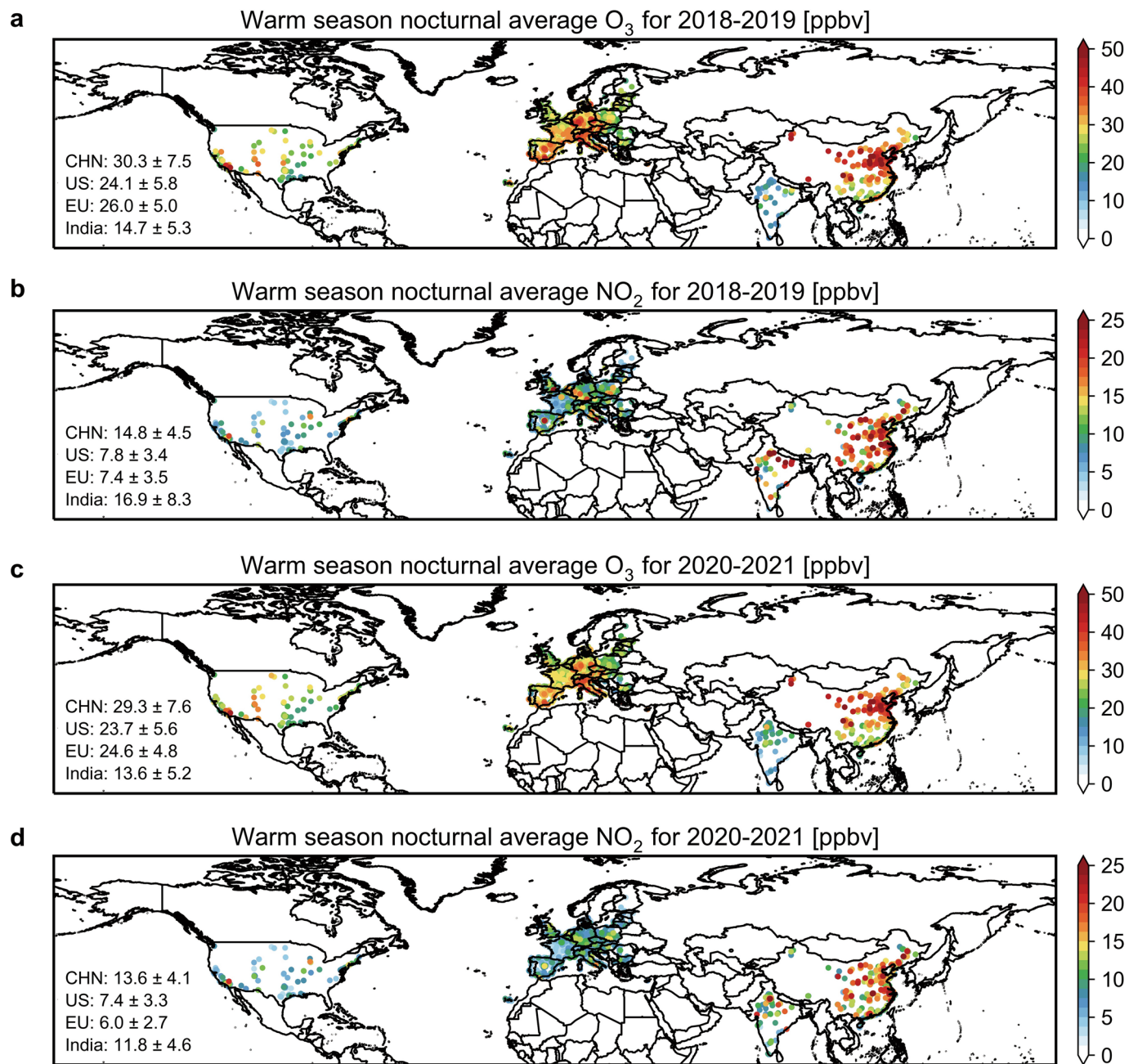
Extended data is available for this paper at <https://doi.org/10.1038/s41561-022-01122-x>.

Supplementary information The online version contains supplementary material available at <https://doi.org/10.1038/s41561-022-01122-x>.

Correspondence and requests for materials should be addressed to Keding Lu, Steven S. Brown or Yuanhang Zhang.

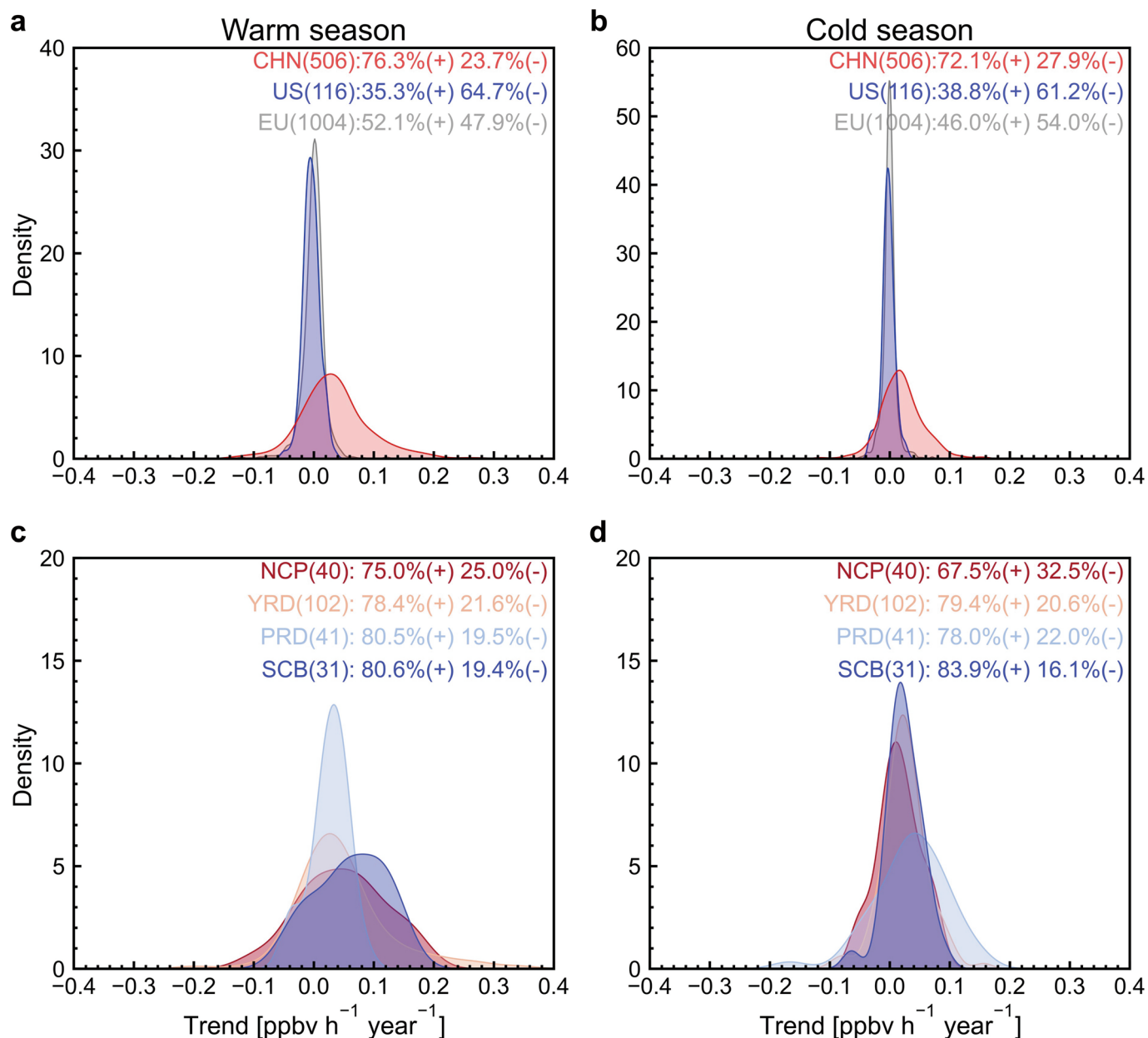
Peer review information *Nature Geoscience* thanks the anonymous reviewers for their contribution to the peer review of this work. Primary Handling Editor: Xujia Jiang, in collaboration with the *Nature Geoscience* team.

Reprints and permissions information is available at www.nature.com/reprints.

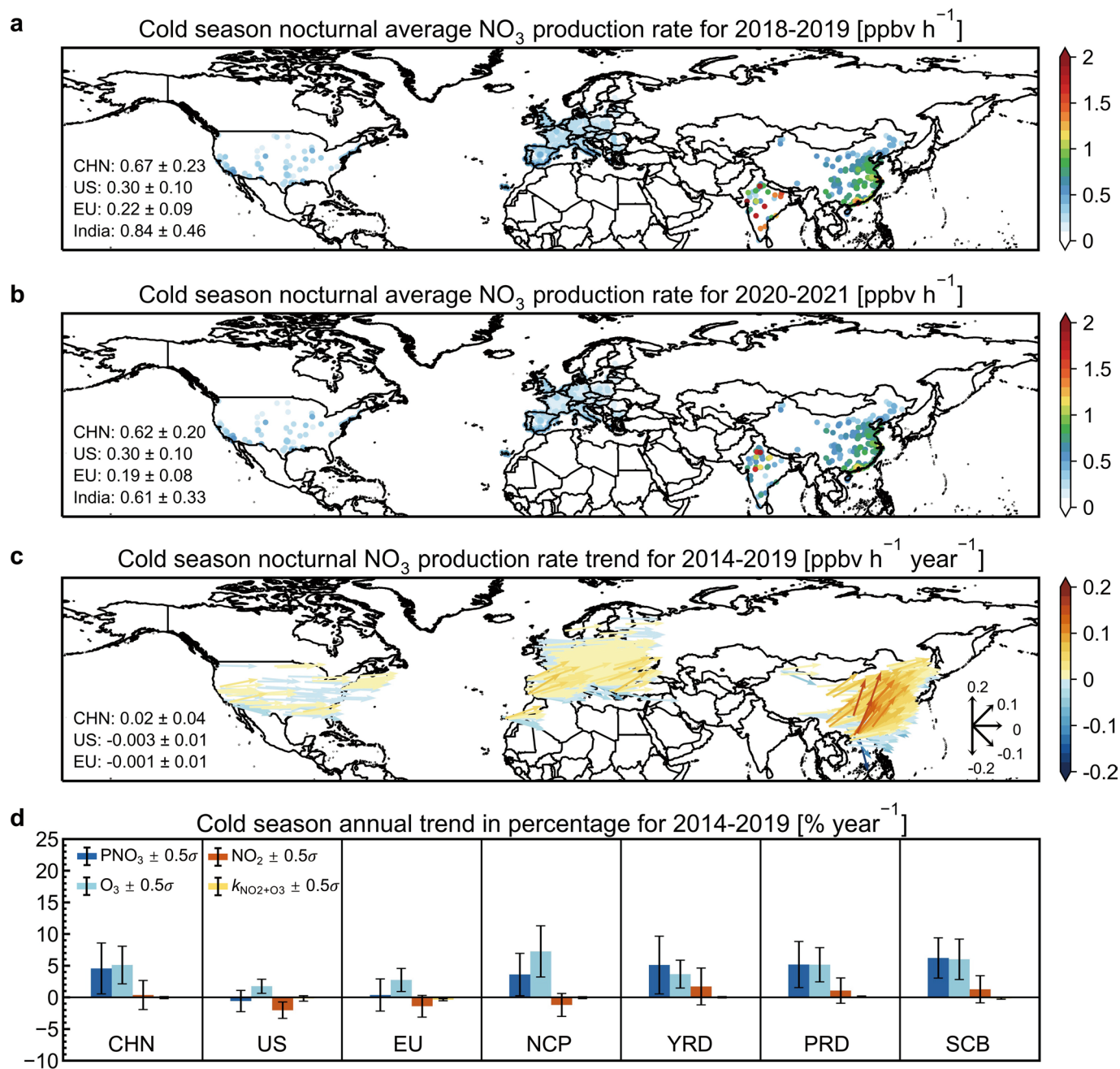


Extended Data Fig. 1 | Average nocturnal O₃ and NO₂ in 2018–2019 and 2020–2021 in warm season. Observed level and trend of nocturnal O₃ and NO₂ in the warm season (April–September). **a,b**, Average nocturnal O₃ (**a**) and NO₂ (**b**) in warm season during 2018–2019. **c,d**, Average nocturnal O₃ (**c**) and NO₂ (**d**) in warm

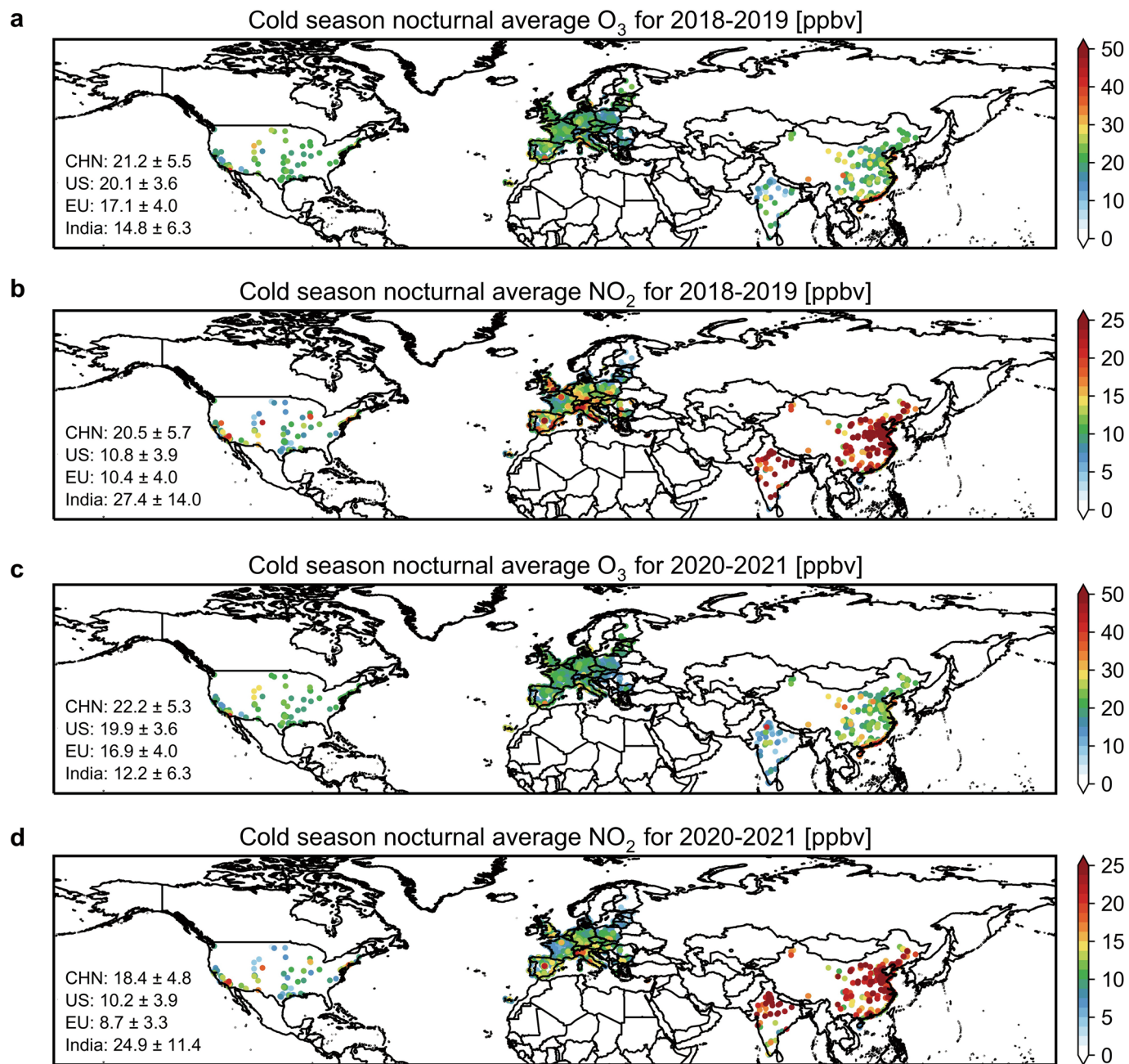
season during 2020–2021. The average \pm standard deviation result in China, the United States, the European Union and India are labelled out in the left in each panel. Basemap reproduced from ref.⁵² under a Creative Commons license CC BY 4.0.



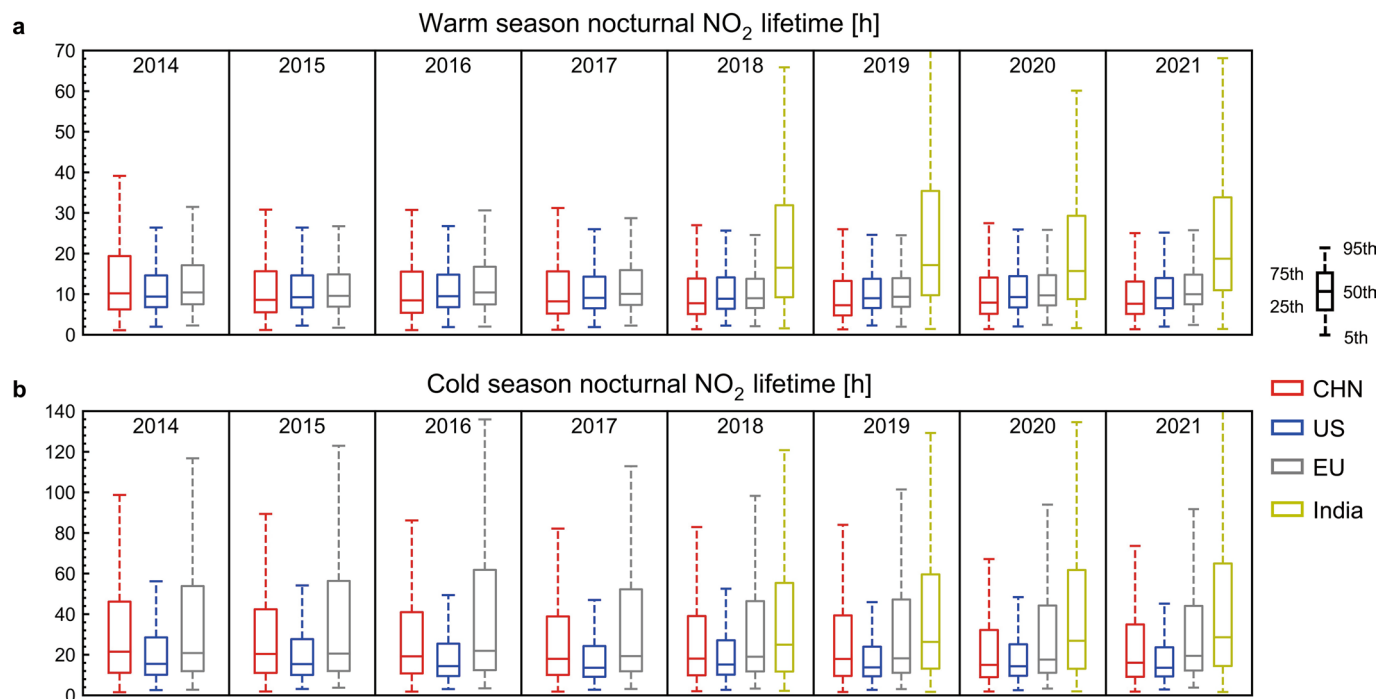
Extended Data Fig. 2 | Histograms of the change rates of PNO₃ during 2014–2019. Site number histograms of the change rates of PNO₃ during 2014–2019 in different seasons and regions. **a, b**, Results of China, the European Union and the United States in warm (**a**) and cold (**b**) seasons. **c, d**, Same as **a** and **b** but for four city clusters in China.



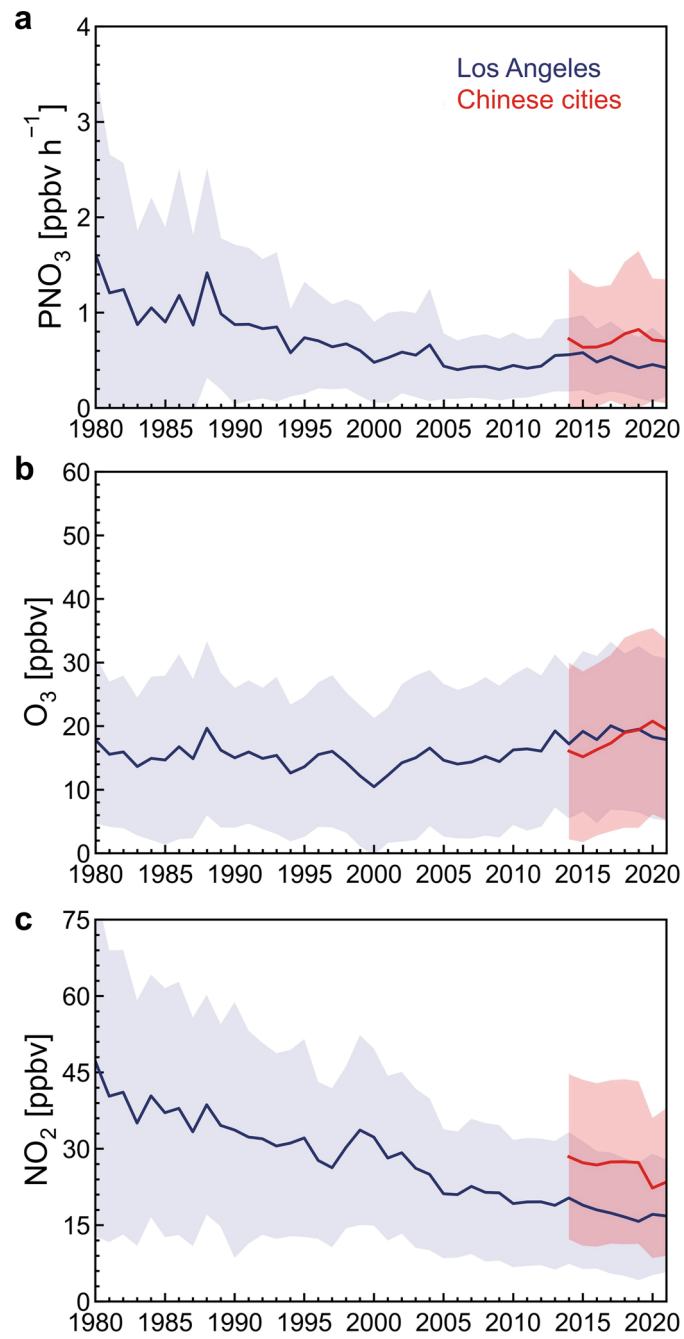
Extended Data Fig. 3 | Observed level and trend of nocturnal nitrate radical production rate (PNO_3) in the cold season (April–September). Same as Fig. 1 but in cold season. Basemap reproduced from ref. ³² under a Creative Commons license CC BY 4.0.



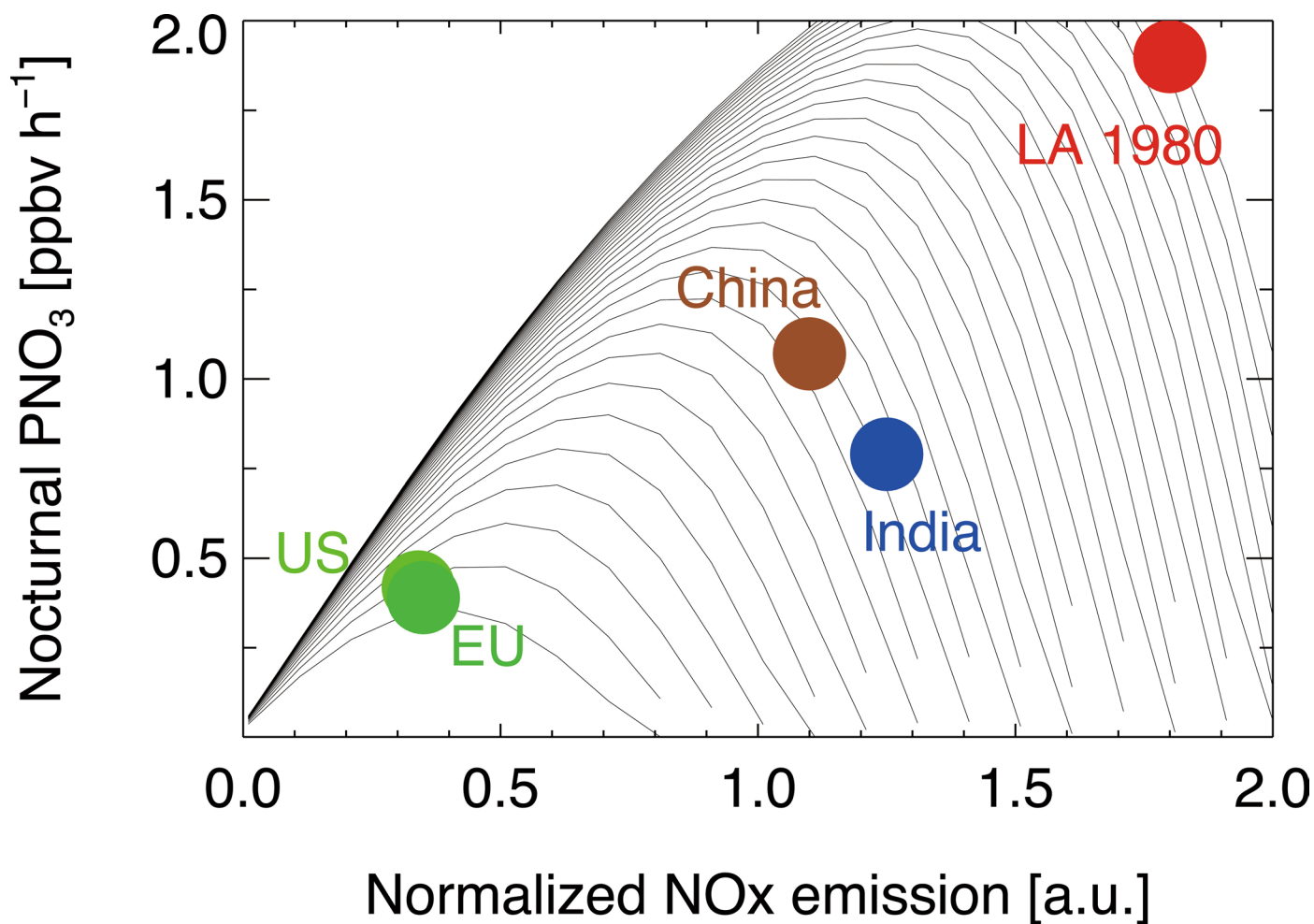
Extended Data Fig. 4 | Average nocturnal O_3 and NO_2 in 2018–2019 and 2020–2021 in cold season. Same as Extended Data Fig. 1. but for cold season. Basemap reproduced from ref.⁵² under a Creative Commons license CC BY 4.0.



Extended Data Fig. 5 | Annual nocturnal lifetime of NO₂. The box whisker of annual nocturnal lifetime of NO₂ in warm. (a), and cold season. (b), in the four regions. More details of the data are listed in Supplementary Table 1.



Extended Data Fig. 6 | The annual trend of nocturnal PNO_3 , NO_2 and O_3 from 1980 to 2021. Same as Fig. 4 but for cold season.



Extended Data Fig. 7 | The nocturnal dependence of PNO₃ on the NO_x emission. The nocturnal NO₃ production rate as functions of the NO_x emission at different VOC level. The dots in different color represent the average condition in the five regions (the United States, the European Union, China and India in 2018–2019 and LA in 1980).

Extended Data Table 1 | The PNO₃, O₃, NO₂, during 2018–2019

Region	Warm season average			Cold season average		
	PNO ₃ [ppbv h ⁻¹]	O ₃ [ppbv]	NO ₂ [ppbv]	PNO ₃ [ppbv h ⁻¹]	O ₃ [ppbv]	NO ₂ [ppbv]
CHN	1.07 ± 0.38	30.3 ± 7.5	14.8 ± 4.5	0.67 ± 0.23	21.2 ± 5.5	20.5 ± 5.7
US	0.42 ± 0.19	24.1 ± 5.7	7.8 ± 3.4	0.30 ± 0.09	20.1 ± 3.6	10.8 ± 3.9
EU	0.39 ± 0.17	26.0 ± 5.0	7.4 ± 3.5	0.22 ± 0.09	17.1 ± 4.0	10.4 ± 4.0
India	0.78 ± 0.50	14.7 ± 5.3	16.9 ± 8.3	0.84 ± 0.50	14.8 ± 6.3	27.4 ± 14.0
NCP	1.56 ± 0.29	40.6 ± 6.5	15.8 ± 4.3	0.70 ± 0.08	19.8 ± 3.6	25.4 ± 4.5
YRD	1.28 ± 0.34	30.5 ± 4.6	16.2 ± 3.7	0.80 ± 0.16	21.4 ± 3.7	23.1 ± 4.4
PRD	0.86 ± 0.19	22.0 ± 3.3	14.0 ± 3.8	1.07 ± 0.21	25.3 ± 4.9	20.5 ± 5.7
SCB	1.09 ± 0.21	28.6 ± 6.2	14.4 ± 3.6	0.57 ± 0.11	17.5 ± 5.2	18.9 ± 4.0

Summary of the PNO₃, O₃ and NO₂ in each region during warm and cold seasons during 2018–2019 (average ± standard deviation)

Extended Data Table 2 | The temperature and the reaction rate constant of NO₂ and O₃ during 2018–2019

Regions	Warm season average		Cold season average	
	T [K]	$k_{NO_2+O_3}$ [10^{-17} s^{-1}]	T [K]	$k_{NO_2+O_3}$ [10^{-17} s^{-1}]
CHN	293.1 ± 4.1	3.1 ± 0.3	278.4 ± 8.1	2.0 ± 0.5
US	291.7 ± 4.0	3.0 ± 0.3	280.0 ± 5.6	2.1 ± 0.3
EU	287.1 ± 2.6	2.6 ± 0.2	277.5 ± 3.9	1.9 ± 0.3
India	299.9 ± 2.1	3.7 ± 0.2	290.5 ± 2.9	2.9 ± 0.2
NCP	292.5 ± 1.5	3.1 ± 0.1	275.3 ± 1.5	1.8 ± 0.1
YRD	294.3 ± 0.8	3.2 ± 0.1	280.5 ± 2.1	2.1 ± 0.1
PRD	298.7 ± 0.8	3.6 ± 0.1	290.4 ± 1.5	2.9 ± 0.1
SCB	294.8 ± 1.0	3.2 ± 0.1	282.0 ± 1.1	2.2 ± 0.1

Summary of the temperature and the reaction rate constant of NO₂ and O₃ in each region during warm and cold seasons during 2018–2019 (average ± standard deviation)

Extended Data Table 3 | The trend PNO₃ and sites distribution in each region during 2014–2019

Region	Warm season		Cold season	
	Linear trend [ppbv h ⁻¹ year ⁻¹]	Positive vs negative sites	Linear trend [ppbv h ⁻¹ year ⁻¹]	Positive vs negative sites
CHN	0.04 ± 0.06	386 vs 120	0.02 ± 0.04	365 vs 141
US	-0.004 ± 0.01	41 vs 75	-0.003 ± 0.01	45 vs 71
EU	-0.0005 ± 0.02	523 vs 481	-0.0008 ± 0.01	462 vs 542
NCP	0.05 ± 0.07	30 vs 10	0.02 ± 0.03	27 vs 13
YRD	0.05 ± 0.08	80 vs 22	0.02 ± 0.04	81 vs 21
PRD	0.03 ± 0.03	33 vs 8	0.03 ± 0.06	32 vs 9
SCB	0.06 ± 0.06	25 vs 6	0.02 ± 0.03	26 vs 5

Summary of the trend PNO₃ and sites distribution in each region during warm and cold seasons during 2014–2019 (average ± standard deviation)